NANO LETTERS

pubs.acs.org/NanoLett

Letter

# Piezotronic Synapse Based on a Single GaN Microwire for Artificial Sensory Systems

Qilin Hua, Xiao Cui, Haitao Liu, Caofeng Pan,* Weiguo Hu,* and Zhong Lin Wang*

Cite This: *Nano Lett.* 2020, 20, 3761−3768

Read Online

ACCESS | Metrics & More | Article Recommendations | Supporting Information

**ABSTRACT:** Tactile information is efficiently captured and processed through a complex sensory system combined with mechanoreceptors, neurons, and synapses in human skin. Synapses are essential for tactile signal transmission between pre/post-neurons. However, developing an electronic device that integrates the functions of tactile information sensation and transmission remains a challenge. Here, we present a piezotronic synapse based on a single GaN microwire that can simultaneously achieve the capabilities of strain sensing and synaptic functions. The piezotronic effect in the wurtzite GaN is introduced to strengthen synaptic weight updates (e.g., 330% enhancement at a compressive stress of −0.36%) with pulse trains. A high gauge factor for strain sensing (ranging from 0 to −0.81%) of about 736 is also obtained. Remarkably, the piezotronic synapse enables the neuromorphic hardware achievement of the perception and processing of tactile information in a single micro/nanowire system, demonstrating an advance in biorealistic artificial intelligence systems.

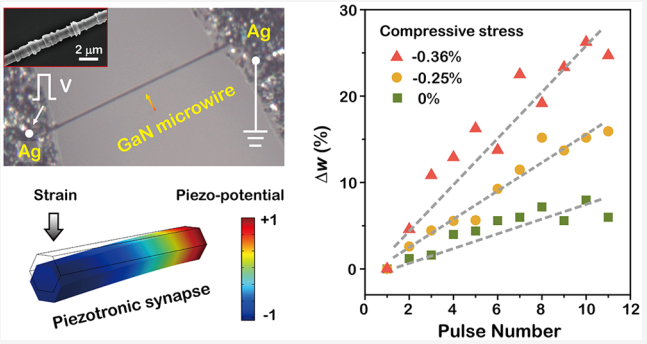


**KEYWORDS:** *GaN, micro/nanowire, piezotronic, synapse, neuromorphic, strain sensing*

Bioinspired electronic systems are driving the rapid development of the fields of artificial intelligence (AI), such as neuromorphic computing,[1,2] humanoid robotics,[3,4] and electronic skins.[5−8] Human skin can efficiently perceive tactile information through a complex sensory system combined with mechanoreceptors, neurons, and synapses. Tactile stimuli are transduced into electrical impulses by various mechanoreceptors (e.g., Merkel's disks). And then, these tactile signals are transmitted via synapses between pre/post-neurons and finally to the central nervous system. In the biological synapse, repeated stimuli can affect the dynamics of $Ca^{2+}$ ions at the biological synapse that leads to changes in synaptic weights.[9] It is remarkable that the synapse and its synaptic weight change is the basis for information processing and transmission. Equivalently, artificial synapse that emulates biosynaptic plasticity functions has been developed into the neuromorphic systems.[9−12] To date, memristors based on metal oxides[9,13,14] or polymers[15,16] are reported to emulate synaptic behaviors and implement artificial neural networks.[13] Furthermore, the development of artificial sensory (or neuromorphic) systems that imitate the sense of touch can benefit from the improved understanding of information processing in somatosensory peripheral nerves. Bao et al. reported a pressure sensor integrated with a ring oscillator and a synaptic transistor to transduce pressure into frequency signals directly.[7,17] Chen et al. presented an artificial sensory neuron, composed of a resistive pressure sensor, a synaptic transistor, and a soft ionic conductor, that can recognize the spatiotemporal features of touched patterns.[18] However, those systems are very complicated in integration and inevitably limit the large-scale applications for future artificial intelligence. Necessarily, a device that can sense, store, and process information with low power consumption is highly desirable for future neuromorphic systems.

Low dimensional piezoelectric semiconductors are very suitable for the design of the artificial sensory systems, due to the piezotronic effect. More specifically, the piezotronic effect, by coupling piezoelectric polarization and semiconductor properties, uses the piezo-potential generated in the piezoelectric semiconductor as a virtual-gate voltage to modulate the interface barrier or control charge carrier transport characteristics for fabricating new devices.[19] That is, strain-induced polarization charges are also capable of tuning channel conductance in such devices, which instead arouses the capability of strain sensing. Also, the piezotronic effect has been demonstrated in wurtzite-structured semiconductors, e.g., ZnO,[20−22] and GaN,[23−25] commonly in direct current mode, and enhanced performance by applying external stress for

Received: February 22, 2020
Revised: April 18, 2020
Published: April 24, 2020

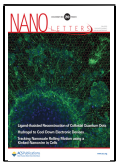







https://dx.doi.org/10.1021/acs.nanolett.0c00733
*Nano Lett.* 2020, 20, 3761−3768

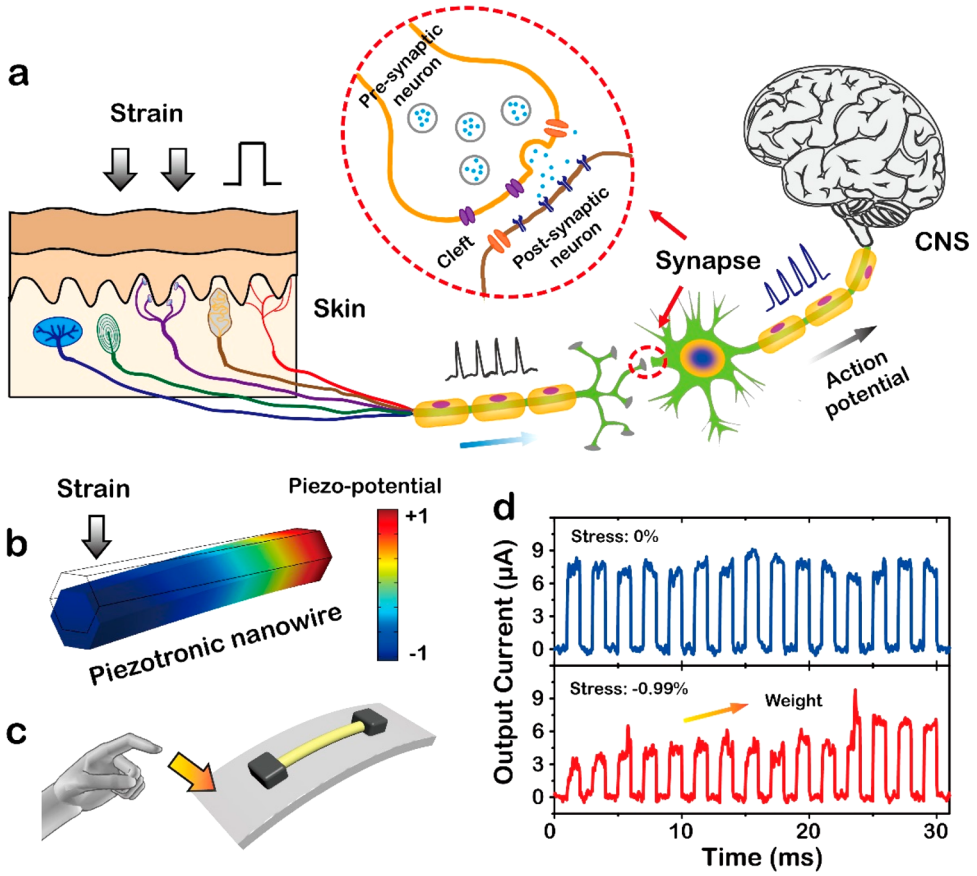


**Figure 1.** Concept of piezotronic synapse. (a) Schematic illustration of mechanosensory and processing via synapse in the biological skin. The red dashed cycle shows the detailed structure of the synapse, composed of pre/post-synaptic neurons and synaptic cleft. (b) The finite element analysis for the piezo-potential distribution of a hexagonal GaN nanowire by applying pressure or strain (COMOSOL Multiphysics). The nanowire device has the potential to couple with the functions of tactile sensing and synaptic characteristics. (c) Schematic illustration of piezotronic synapse based on a single GaN micro/nanowire. (d) The changes in current (synaptic weight) without (top) or with (bottom) compressive stress by applying the same pulse trains (2 V, 1 ms). Under stress of −0.99%, the synaptic weight shows a remarkable increase with pulse trains.

various piezotronic devices, including sensors,[21,26] photodetectors,[27,28] LEDs,[22,29] solar cells,[30,31] lasers,[32] memristors,[23,33] and power devices,[34] has been widely reported. More impressively, one-dimensional GaN nanostructures, e.g., nanowires[25] and nanobelts,[33] have great application prospects for information storage[23] and piezotronic modulation.[33]

Here, we present a piezotronic synapse fabricated in a single GaN microwire that can simultaneously achieve the capabilities of tactile sensation and transmission. Such a device design based on a single GaN micro/nanowire contributes to the reduction of the artificial sensory system complexity. Threshold switching behavior and short-term plasticity synaptic functions are demonstrated in the device. More importantly, the piezotronic effect in pulse (or alternating current) mode is introduced to strengthen synaptic weight updates through effective electrons transport modulation in the wurtzite GaN-based device. The device also provides strain sensing with a gauge factor as high as 736, by monitoring the synaptic weight enhancement with compressive stress.

Figure 1a illustrates a schematic of mechanosensation and the related signal processing via synapse in the biological skin. External mechanical stimuli (e.g., pressure, stress, and torsion) can excite various mechanoreceptors (e.g., Merkel's disks) to produce electrical impulses (i.e., action potentials) which carry the tactile information in the form of temporal signals. Synapses act as information conveyers that can either excite or inhibit the postsynaptic neuron via neurotransmitters, as schematically shown in the inset of Figure 1a. A hexagonal GaN nanowire is capable of generating piezo-potential by applying pressure or strain due to the piezoelectric polarization, which is simulated by COMSOL Multiphysics (Figure 1b). More impressively, the micro/nanowire device has the potential to couple with the functions of tactile sensing and synaptic behaviors, which we call "piezotronic synapse". Figure 1c shows a schematic of piezotronic synapse based on a single GaN microwire, illustrating a very promising building block for the artificial sensory systems and human−machine interfaces. Furthermore, the change in synaptic weight can be tuned by applying a compressive stress with voltage pulse trains (2 V, 1 ms), as shown in Figure 1d. The output current (or synaptic weight) has no great changes under the stress-free condition. However, when applying a compressive stress of −0.99%, the synaptic weight shows a remarkable increase with pulse trains. It means that the updates of the synaptic weight can be controlled by external mechanical stimuli under the piezotronic effect in pulse mode. From another perspective, the condition of stress loading can also be obtained according to the change in synaptic weight.

Figure 2a illustrates the device structure of the GaN microwire based piezotronic synapse. The single GaN microwire was synthesized by a chemical vapor deposition (CVD) method, transferred onto a polystyrene (PS) substrate,


https://dx.doi.org/10.1021/acs.nanolett.0c00733
Nano Lett. 2020, 20, 3761−3768

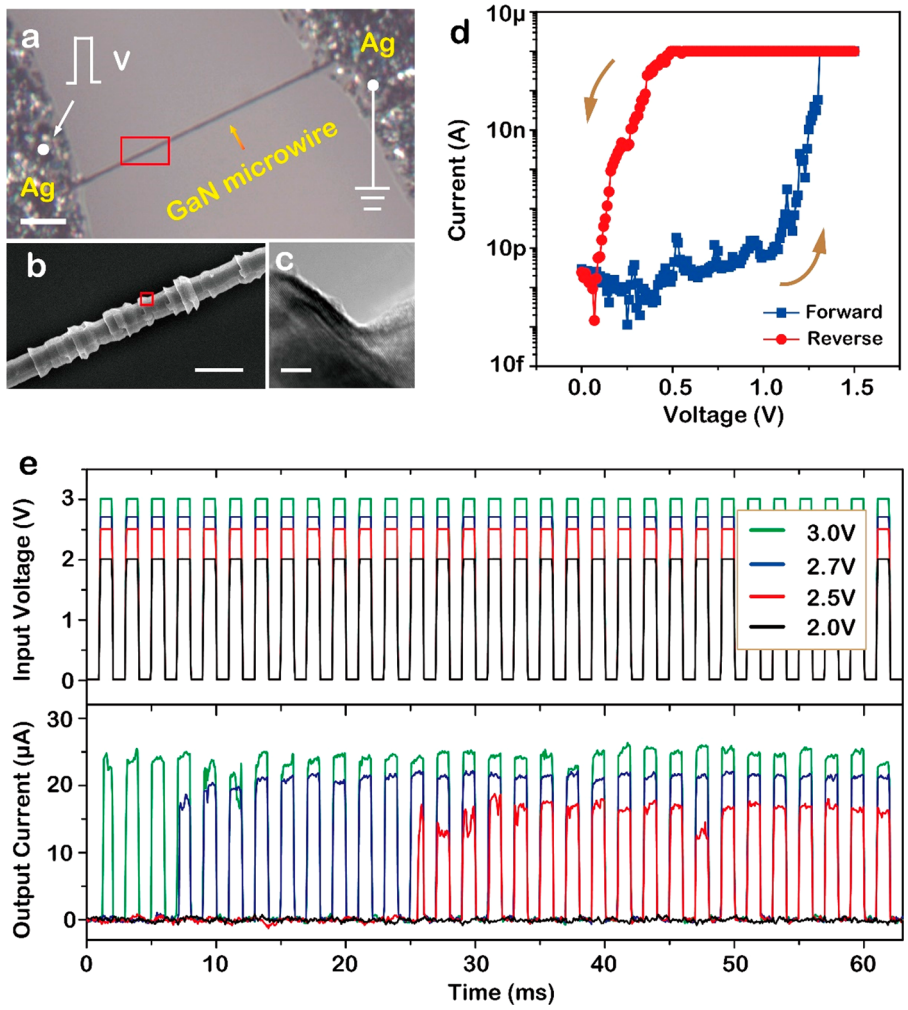


**Figure 2.** GaN microwire based piezotronic synapse. (a) Optical image of the device with the structure of Ag/GaN microwire/Ag. Scale bar: 20 $\mu$m. (b) Scanning electron microscopy (SEM) image of the GaN microwire, showing the bamboo-shaped structure. Scale bar: 2 $\mu$m. (c) Transmission electron microscopy (TEM) image of the GaN microwire at the knot. Scale bar: 5 nm. (d) Typical DC $I-V$ characteristics of the GaN microwire device, including forward (blue) and reverse (red) voltage sweeping, under a compliance current ($I_{cc}$) of 1 $\mu$A. (e) Response of the GaN microwire device to input voltage pulse trains. The top shows the pulse trains (1 ms, 31 pulses) with different voltage amplitudes (2.0, 2.5, 2.7, and 3.0 V). The bottom shows the output current response to the input trains. The currents are observed to be switching-on when the voltage amplitude ≥2.5 V. The incubation time, which indicates the number of pulses for the switching event, is shorten with the increase of the pulse amplitude. The pulse trains with the pulse amplitude of 3 V could contribute to the formation of a large conductive channel, resembling the forming process and inducing more $V_N$ trap states.

and followed by forming source/drain contacts with a silver paste. A bamboo-shaped GaN microwire is observed in the scanning electron microscopy (SEM) images of Figures S1 and 2b, and the knot of the GaN microwire is shown in the transmission electron microscopy (TEM) image of Figure 2c. The single-crystal GaN microwire grows along the *c*-axis, according to our previous report.[23] Micro-Raman scattering of the GaN microwire on the PS substrate is shown in Figure S2. The shifts at 566.9, 557.2, and 529.9 $cm^{-1}$ are respectively identified as the $E_2$(high), $E_1$(TO), and $A_1$(TO) modes of GaN. Based on the symmetric and strong phonon line of $E_2$(high) at 566.9 $cm^{-1}$, it can be found that the GaN microwire is high crystallinity and shows hexagonal phase characteristics. The typical DC $I-V$ characteristics of the GaN microwire device at forward/reverse voltage sweeping under a compliance current ($I_{cc}$) of 1 $\mu$A are shown in Figure 2d. When the applied voltage is larger than the threshold voltage ($V_{th}$), the device abruptly switches on and the current increases to the $I_{cc}$ level (at low resistance state, LRS) at forward voltage sweeping; when the applied voltage reduces to below the hold voltage ($V_{hold}$), the device spontaneously switches off and the current decreases back to the level of 1 pA (at high resistance state, HRS). That is, the threshold switching behavior of the piezotronic synapse is clearly demonstrated.

The control of resistance states in the synapses by applying pulses is of great importance to implement neuromorphic functions.[35] By using voltage train pulses as the input stimuli, the dynamics of the piezotronic synapse is systemically investigated to demonstrate the features of the implementation of neuromorphic hardware. The switching characteristics of the piezotronic synapse is highly dependent on the number, amplitude, or width of train pulses. In Figure 2e, the output currents are clearly recorded when input pulse trains (1 ms, 31 pulses) with various voltage amplitudes (2.0, 2.5, 2.7, and 3.0 V). Below a critical pulse voltage amplitude (<2.5 V), pulse trains do not lead to a change in conductance of the device. However, the increased conductance (or current jump) is observed when the train pulse voltage is ≥2.5 V. The similar


https://dx.doi.org/10.1021/acs.nanolett.0c00733
Nano Lett. 2020, 20, 3761−3768

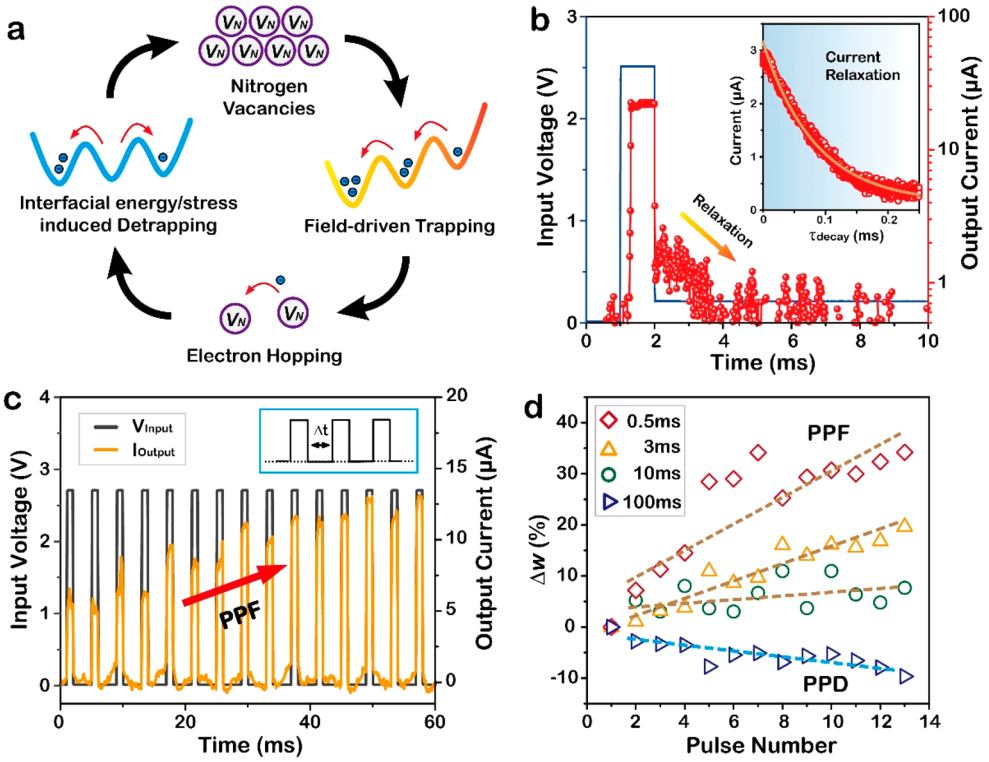


**Figure 3.** Short-term plasticity of the GaN microwire device. (a) The mechanism illustration for the procedures of field-driven trapping and interfacial energy/stress induced detrapping. (b) The temporal response to an input voltage pulse (1 ms, 2.5 V). The inset shows the current relaxation (decay) process after the device switching off (also shown in Figure S5). The relaxation (or decay time, $\tau_{delay}$) can be tuned from 3 $\mu$s to 2 ms via a controlled voltage pulse. (c) Paired-pulse facilitation (PPF) characteristic demonstration. The current response (orange) to the input voltage pulse trains (2.7 V, 1 ms, 15 pulses). The inset blue rectangle shows the scheme of the pulse trains with 1 ms pulse time and 3 ms interval time ($\Delta t$). (d) The change in conductance (synaptic weight, $\Delta w$) as a function of pulse number (2.7 V, 1 ms) with different $\Delta t$ (0.5, 3, 10, and 100 ms), demonstrating the PPF and PPD characteristics. A shorter $\Delta t$ leads to a larger percentage of $\Delta w$ change, which will turn to be negative when the $\Delta t$ reaches 100 ms.

process of pulse response is also represented at the top of Figure S3. Moreover, the incubation time, which indicates the number of pulses for the switching event, is shorten with the increase of the pulse amplitude, and the current jumps at the first applied pulse when the pulse amplitude is $\geq$3 V. Additionally, the current jumps come to occur, and the incubation time can be reduced, when consecutively applying a small pulse amplitude of 2 V by modulating the pulse width (from 0.5 to 10 ms), as shown in the bottom of Figure S3.

The dynamics of $Ca^{2+}$, including the procedures of influx and extrusion, in the pre/post-synaptic neuron are essentially critical for the change of plasticity in the biological synapse.[9] Based on the fitting $I-V$ plot of the GaN microwire device in Figure S4, the trap-controlled space-charge-limited-conduction (SCLC) theory[36] can be used to explain the conduction mechanism. A large number of trap states (e.g., nitrogen vacancies) are initially formed in the bamboo-shaped GaN microwire, probably at the knots,[23] due to applying a compressive stress of −1.43% at first. The nitrogen vacancies ($V_N$) in the GaN microwire acting as trap states that can contribute to the formation of conductive channel with electrons trapping and detrapping procedures,[37,38] which is analogous to the dynamics of $Ca^{2+}$ in the biological synapse. Figure 3a illustrates the detailed electrons trapping/detrapping in the GaN microwire device. The procedures of trapping and detrapping indicate the switching on/off-state of the GaN microwire device, respectively. More specifically, electrons are easily driven into the unfilled-traps by applying an electric field (i.e., trapping), while they could escape from the filled-traps due to the interfacial energy or stress effect (i.e., detrapping).[36−38] In addition, the conductance increases with pulse trains in an abrupt manner (Figure 2e). A large conductive channel can be formed under the sufficient pulse amplitude of 3 V, resembling the forming process and inducing more $V_N$ trap states. After that, when applying pulse trains with a pulse amplitude of 2.5 or 2.7 V again (Figure 3b−d), the conductance appears to jump at the first applied pulse and also shows a gradual increase with pulse trains under the effects of Joule heat,[39,40] interfacial energy or stress, and an electric field.

Furthermore, the dynamical characteristics of the GaN microwire device are investigated by using voltage pulse input. As shown in Figure 3b, upon applying a voltage pulse (1 ms, 2.5 V), the GaN microwire device comes to show the resistance transition to LRS with an incubation procedure, which is induced by the field-driven electrons trapping through the nitrogen vacancies. After the pulse voltage decreases to 0.1 V, the device exhibits the relaxation back to HRS over a decay time ($\tau_{decay}$), as a result of detrapping induced by the interfacial energy or stress effect. The current relaxation curve can be well fitted by using the basic exponential function (the inset of Figure 3b): $I(t) = I_0 + \alpha \times \exp(-t/\tau_{decay})$, where $I(t)$ and $I_0$ are the corresponding currents at the time of $t$ and the original state, respectively, and $\alpha$ is a factor constant. The current relaxation process is also presented by a triangle pulse (2 ms, 4 V) on the device in Figure S5. The $\tau_{delay}$ can be effectively


https://dx.doi.org/10.1021/acs.nanolett.0c00733
Nano Lett. 2020, 20, 3761−3768

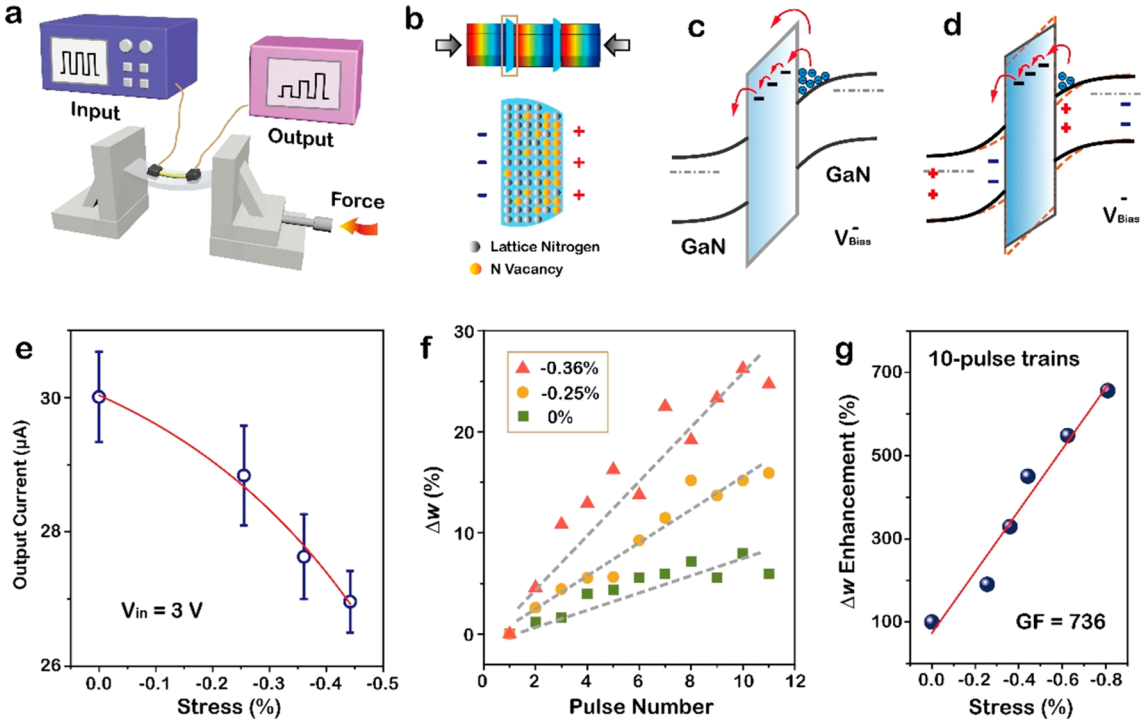


**Figure 4.** Piezotronic modulated plasticity of the GaN microwire device. (a) Schematic illustration for piezotronic measurement of the device. With applying compressive stress on the device, the change in output current can be monitored as the input voltage pulse trains. (b) Schematic illustration for the nitrogen vacancies ($V_N$) at the knot of the GaN microwire can be controlled with the applied compressive stress. (c, d) The band diagrams of the device without/with compressive stress in piezotronic effect, respectively. (e) The output currents response to different compressive stress (from 0 to −0.44%), when the input voltage pulse ($V_{in}$) is 3 V. (f) The synaptic weight change as a function of pulse number (2.7 V, 1 ms; $\Delta t$: 3 ms) with different compressive stress (0%, −0.25%, and −0.36%). Larger stress could result in a larger percentage of $\Delta w$ change. (g) The $\Delta w$ enhancement significantly increases with the increase of the applied compressive stress (from 0% to −0.81%) after input 10-pulse trains. As it derived, the gauge factor (GF) for strain sensing is as high as 736.

tuned from 3-$\mu$s-scale to 2 ms-scale by controlling the pulse parameters including voltage bias and duration time, which is in analogy to the response dynamics of short-term plasticity of the biological synapse.

The paired-pulse facilitation (PPF) (or paired-pulse depression, PPD) characteristic is one of the key features in the biological synapse, and the synaptic strength will be temporally enhanced (or reduced) with repeated stimuli. Figure 3c demonstrates the PPF characteristic of the piezotronic synapse. The output conductance (i.e., synaptic weight, $\Delta w$) of the GaN microwire device obviously shows an increase by applying pulse trains of 1 ms pulse time and 3 ms interval time ($\Delta t$). The frequency of applied pulses (i.e., different period of $\Delta t$) to synapses can induce an increase or decrease in postsynaptic responses, leading to PPF or PPD in short-term plasticity.[9,35] When $\Delta t$ is short (e.g., 0.5−10 ms), the output conductance increases from the original state with the increase of pulse trains, demonstrating PPF, and the conductance could significantly increase by about 7 times as reducing the $\Delta t$ from 10 to 0.5 ms. Conversely, a long $\Delta t$ (e.g., 100 ms) would lead to a decrease of conductance in pulse trains (exhibiting PPD), due to the relaxation behavior of the device at low-frequency stimulation. Furthermore, when a stimulus is temporarily stored in the short term memory, the information will be forgotten or permanently transferred to the long-term memory with a process of rehearsal.[42] Figure S6 illustrates short-term to long-term potentiation transition of the GaN microwire device with two repeated pulse trains. Although its conductance has a certain degree of decay both after first and second pulse trains, the device shows the possibility of long-term potentiation with the repeated rehearsal trains. Resembling the biological synapse, the GaN microwire device is capable to emulate multiple synaptic functions, such as PPF and PPD, and will be suitable for tactile or related signal processing.

GaN is a kind of typical piezotronic material, which has coupling effects of semiconductor and piezoelectric properties, so it will extend the applications including electrical and mechanical performance. And thus, the GaN microwire device has a unique capability of strain sensing, except for emulating the biological synaptic functions, due to the piezotronic effect. To elucidate the piezotronic effect in the GaN microwire-based synapse, we establish a homemade testing setup composed of a stress loading apparatus and a semiconductor tester with a pulse module, as schematically shown in Figure 4a. The change in synaptic weight can be monitored in real-time with the input voltage pulse trains under stress-free or stress conditions. That is, the piezotronic effect of the GaN microwire device is investigated in the pulse mode. Figure 4b illustrates the mechanism of the piezotronic synapse. The nitrogen vacancies ($V_N$) at the knot of the device can be controlled by the piezo-potential induced by the applied compressive stress and redistribute at the positive charge side, which may affect the synaptic behavior of the GaN microwire device. The band diagrams of the device without/with the compressive stress are shown in Figures 4c and 4d, respectively, to further understand the mechanism. The knot region filled with a large number of $V_N$ is considered as a


https://dx.doi.org/10.1021/acs.nanolett.0c00733
Nano Lett. 2020, 20, 3761−3768

variable barrier,[23,41] and the $V_N$ acting as traps contribute to the transport of electrons. Under a voltage bias, the band is inclined to be tilted, and electrons would accumulate at the interface of the knot, which will transport via thermal emission or tunneling (Figure 4c). By applying a compressive stress, the tilted band is compensated by the introduced piezo-potential due to the piezotronic effect (Figure 4d). The accumulation and transport of electrons are also decreased. By using another applying voltage strategy, i.e., input pulses, we may be able to more clearly understand the process of the accumulation and transport of electrons under the piezo-potential. The output current shows a decrease in response to different compressive stress (from 0 to −0.44%), as shown in Figure 4e, which is consistent with the analysis of the band diagram on the piezotronic effect. The synaptic weight updates as a function of pulse number (2.7 V, 1 ms; $\Delta t$: 3 ms) with different compressive stress (0%, −0.25%, and −0.36%) are illustrated in Figure 4f. Loading a larger stress could lead to a larger percentage of $\Delta w$ change. Specifically, the synaptic weight shows a pronounced enhancement of 330% with the increase of the compressive stress from 0% to −0.36%, as a result of effective electrons transport modulation by the piezotronic effect in pulse mode. To think from another point of view, the piezotronic synapse has a capability for strain sensing and can act as a strain sensor. By increasing the applied compressive stress from 0 to −0.81%, the $\Delta w$ enhancement shows a nearly linear increase by 6.5 times after input 10-pulse trains, as shown in Figure 4g. Based on monitoring the $\Delta w$ enhancement, we can directly obtain the compressive stress condition, and the gauge factor (GF) for strain sensing (ranging from 0 to −0.81%) is as high as 736.

In summary, a single GaN microwire-based piezotronic synapse can simultaneously achieve the capabilities of tactile sensation and transmission, which is very significant to simplify the complexity of the artificial sensory system. The device exhibits the threshold switching behavior and emulates the short-term synaptic functions of the biological synapse, as well as low energy consumption (Figure S7). The dynamics of the device is considered such that nitrogen vacancies acting as electron traps contribute to the formation of electron transport channels at the knots of the bamboo-shaped GaN microwire. Under the piezotronic effect of the wurtzite GaN with inputting pulses, the device can be used to strengthen synaptic weight updates (e.g., 330% enhancement at a compressive stress of −0.36%) and provide a high gauge factor for strain sensing of about 736. Looking forward, the piezotronic synapse enables the neuromorphic hardware achievement of the perception and transmission of tactile information in a single micro/nanowire system, demonstrating an advance in biorealistic artificial intelligence systems.

## ■ ASSOCIATED CONTENT

### Supporting Information

The Supporting Information is available free of charge at https://pubs.acs.org/doi/10.1021/acs.nanolett.0c00733.

Experimental methods; SEM images and micro-Raman scattering of CVD-synthesized GaN microwires; pulse response, the double-logarithm $I-V$ plot, and switching characteristic of the GaN microwire device; short-term to long-term potentiation transition; and illustration for energy consumption in various synapses (PDF)

## ■ AUTHOR INFORMATION


### Corresponding Authors

**Caofeng Pan** − *CAS Center for Excellence in Nanoscience, Beijing Key Laboratory of Micro-nano Energy and Sensor, Beijing Institute of Nanoenergy and Nanosystems, Chinese Academy of Sciences, Beijing 100083, China; School of Nanoscience and Technology, University of Chinese Academy of Sciences, Beijing 100049, China; College of Physics and Optoelectronic Engineering, Shenzhen University, Shenzhen 518060, China; Center on Nanoenergy Research, School of Physical Science and Technology, Guangxi University, Nanning, Guangxi 530004, China;* orcid.org/0000-0001-6327-9692; Email: cfpan@binn.cas.cn

**Weiguo Hu** − *CAS Center for Excellence in Nanoscience, Beijing Key Laboratory of Micro-nano Energy and Sensor, Beijing Institute of Nanoenergy and Nanosystems, Chinese Academy of Sciences, Beijing 100083, China; School of Nanoscience and Technology, University of Chinese Academy of Sciences, Beijing 100049, China; Center on Nanoenergy Research, School of Physical Science and Technology, Guangxi University, Nanning, Guangxi 530004, China;* orcid.org/0000-0002-8614-0359; Email: huweiguo@binn.cas.cn

**Zhong Lin Wang** − *CAS Center for Excellence in Nanoscience, Beijing Key Laboratory of Micro-nano Energy and Sensor, Beijing Institute of Nanoenergy and Nanosystems, Chinese Academy of Sciences, Beijing 100083, China; School of Nanoscience and Technology, University of Chinese Academy of Sciences, Beijing 100049, China; School of Materials Science and Engineering, Georgia Institute of Technology, Atlanta, Georgia 30332-0245, United States;* orcid.org/0000-0002-5530-0380; Email: zhong.wang@mse.gatech.edu

### Authors

**Qilin Hua** − *CAS Center for Excellence in Nanoscience, Beijing Key Laboratory of Micro-nano Energy and Sensor, Beijing Institute of Nanoenergy and Nanosystems, Chinese Academy of Sciences, Beijing 100083, China; School of Nanoscience and Technology, University of Chinese Academy of Sciences, Beijing 100049, China;* orcid.org/0000-0002-5269-5532

**Xiao Cui** − *CAS Center for Excellence in Nanoscience, Beijing Key Laboratory of Micro-nano Energy and Sensor, Beijing Institute of Nanoenergy and Nanosystems, Chinese Academy of Sciences, Beijing 100083, China; School of Nanoscience and Technology, University of Chinese Academy of Sciences, Beijing 100049, China*

**Haitao Liu** − *CAS Center for Excellence in Nanoscience, Beijing Key Laboratory of Micro-nano Energy and Sensor, Beijing Institute of Nanoenergy and Nanosystems, Chinese Academy of Sciences, Beijing 100083, China*

Complete contact information is available at: https://pubs.acs.org/10.1021/acs.nanolett.0c00733


### Notes

The authors declare no competing financial interest.

## ■ ACKNOWLEDGMENTS

The authors are thankful for the support from the National Key Research and Development Program of China (2016YFA0202703), the National Natural Science Foundation of China (61904012, 51432005, 61574018, 61704008, 51622205, 61675027, 51432005, 61505010, and 51502018), the Beijing City Committee of Science and Technology

(Z171100002017019 and Z181100004418004), the Natural Science Foundation of Beijing Municipality (4204114, 4181004, 4182080, 4184110, 2184131, and Z180011), the "Hundred Talents Program" of the Chinese Academy of Science, and the University of Chinese Academy of Sciences.

## REFERENCES

(1) Chen, Y.; Li, H.; Wu, C.; Song, C.; Li, S.; Min, C.; Cheng, H.-P.; Wen, W.; Liu, X. Neuromorphic Computing's Yesterday, Today, and Tomorrow - an Evolutional View. *Integration* **2018**, *61*, 49−61.

(2) Burr, G. W.; Shelby, R. M.; Sebastian, A.; Kim, S.; Kim, S.; Sidler, S.; Virwani, K.; Ishii, M.; Narayanan, P.; Fumarola, A.; Sanches, L. L.; Boybat, I.; Le Gallo, M.; Moon, K.; Woo, J.; Hwang, H.; Leblebici, Y. Neuromorphic Computing Using Non-Volatile Memory. *Advances in Physics: X* **2017**, *2*, 89−124.

(3) Boutry, C. M.; Negre, M.; Jorda, M.; Vardoulis, O.; Chortos, A.; Khatib, O.; Bao, Z. A Hierarchically Patterned, Bioinspired E-Skin Able to Detect the Direction of Applied Pressure for Robotics. *Sci. Robot.* **2018**, *3*, No. eaau6914.

(4) Ijspeert, A. Biorobotics: Using Robots to Emulate and Investigate Agile Locomotion. *Science* **2014**, *346*, 196−203.

(5) Chortos, A.; Liu, J.; Bao, Z. Pursuing Prosthetic Electronic Skin. *Nat. Mater.* **2016**, *15*, 937−950.

(6) Wang, S.; Xu, J.; Wang, W.; Wang, G. N.; Rastak, R.; Molina-Lopez, F.; Chung, J. W.; Niu, S.; Feig, V. R.; Lopez, J.; Lei, T.; Kwon, S. K.; Kim, Y.; Foudeh, A. M.; Ehrlich, A.; Gasperini, A.; Yun, Y.; Murmann, B.; Tok, J. B.; Bao, Z. Skin Electronics from Scalable Fabrication of an Intrinsically Stretchable Transistor Array. *Nature* **2018**, *555*, 83−88.

(7) Tee, B. C.; Chortos, A.; Berndt, A.; Nguyen, A. K.; Tom, A.; McGuire, A.; Lin, Z. C.; Tien, K.; Bae, W. G.; Wang, H.; Mei, P.; Chou, H. H.; Cui, B.; Deisseroth, K.; Ng, T. N.; Bao, Z. A Skin-Inspired Organic Digital Mechanoreceptor. *Science* **2015**, *350*, 313−316.

(8) Hua, Q.; Sun, J.; Liu, H.; Bao, R.; Yu, R.; Zhai, J.; Pan, C.; Wang, Z. L. Skin-Inspired Highly Stretchable and Conformable Matrix Networks for Multifunctional Sensing. *Nat. Commun.* **2018**, *9*, 244.

(9) Wang, Z.; Joshi, S.; Savel'ev, S. E.; Jiang, H.; Midya, R.; Lin, P.; Hu, M.; Ge, N.; Strachan, J. P.; Li, Z.; Wu, Q.; Barnell, M.; Li, G. L.; Xin, H. L.; Williams, R. S.; Xia, Q.; Yang, J. J. Memristors with Diffusive Dynamics as Synaptic Emulators for Neuromorphic Computing. *Nat. Mater.* **2017**, *16*, 101−108.

(10) Yu, S. Neuro-inspired Computing with Emerging Nonvolatile Memorys. *P. Proc. IEEE* **2018**, *106*, 260−285.

(11) Zidan, M. A.; Strachan, J. P.; Lu, W. D. The Future of Electronics Based on Memristive Systems. *Nat. Electron.* **2018**, *1*, 22−29.

(12) Hua, Q.; Wu, H.; Gao, B.; Zhang, Q.; Wu, W.; Li, Y.; Wang, X.; Hu, W.; Qian, H. Low-Voltage Oscillatory Neurons for Memristor-Based Neuromorphic Systems. *Global Challenges* **2019**, *3*, 1900015.

(13) Yao, P.; Wu, H.; Gao, B.; Eryilmaz, S. B.; Huang, X.; Zhang, W.; Zhang, Q.; Deng, N.; Shi, L.; Wong, H. P.; Qian, H. Face Classification Using Electronic Synapses. *Nat. Commun.* **2017**, *8*, 15199.

(14) Hua, Q.; Wu, H.; Gao, B.; Zhao, M.; Li, Y.; Li, X.; Hou, X.; Marvin Chang, M.-F.; Zhou, P.; Qian, H. A Threshold Switching Selector Based on Highly Ordered Ag Nanodots for X-Point Memory Applications. *Adv. Sci.* **2019**, *6*, 1900024.

(15) van de Burgt, Y.; Melianas, A.; Keene, S. T.; Malliaras, G.; Salleo, A. Organic Electronics for Neuromorphic Computing. *Nat. Electron.* **2018**, *1*, 386−397.

(16) van de Burgt, Y.; Lubberman, E.; Fuller, E. J.; Keene, S. T.; Faria, G. C.; Agarwal, S.; Marinella, M. J.; Alec Talin, A.; Salleo, A. A Non-Volatile Organic Electrochemical Device as a Low-Voltage Artificial Synapse for Neuromorphic Computing. *Nat. Mater.* **2017**, *16*, 414−418.

(17) Kim, Y.; Chortos, A.; Xu, W.; Liu, Y.; Oh, J. Y.; Son, D.; Kang, J.; Foudeh, A. M.; Zhu, C.; Lee, Y.; Niu, S.; Liu, J.; Pfattner, R.; Bao, Z.; Lee, T.-W. A Bioinspired Flexible Organic Artificial Afferent Nerve. *Science* **2018**, *360*, 998−1003.

(18) Wan, C.; Chen, G.; Fu, Y.; Wang, M.; Matsuhisa, N.; Pan, S.; Pan, L.; Yang, H.; Wan, Q.; Zhu, L.; Chen, X. An Artificial Sensory Neuron with Tactile Perceptual Learning. *Adv. Mater.* **2018**, *30*, No. 1801291.

(19) Wu, W.; Wang, Z. L. Piezotronics and Piezo-Phototronics for Adaptive Electronics and Optoelectronics. *Nat. Rev. Mater.* **2016**, *1*, 16031.

(20) Wang, Z. L.; Song, J. Piezoelectric Nanogenerators Based on Zinc Oxide Nanowire Arrays. *Science* **2006**, *312*, 242−246.

(21) Wang, X.; Zhou, J.; Song, J.; Liu, J.; Xu, N.; Wang, Z. L. Piezoelectric Field Effect Transistor and Nanoforce Sensor Based on a Single Zno Nanowire. *Nano Lett.* **2006**, *6*, 2768−2772.

(22) Pan, C.; Dong, L.; Zhu, G.; Niu, S.; Yu, R.; Yang, Q.; Liu, Y.; Wang, Z. L. High-Resolution Electroluminescent Imaging of Pressure Distribution Using a Piezoelectric Nanowire LED Array. *Nat. Photonics* **2013**, *7*, 752−758.

(23) Liu, H.; Hua, Q.; Yu, R.; Yang, Y.; Zhang, T.; Zhang, Y.; Pan, C. A Bamboo-Like GaN Microwire-Based Piezotronic Memristor. *Adv. Funct. Mater.* **2016**, *26*, 5307−5314.

(24) Du, C.; Hu, W.; Wang, Z. L. Recent Progress on Piezotronic and Piezo-Phototronic Effects in III-Group Nitride Devices and Applications. *Adv. Eng. Mater.* **2018**, *20*, 1700760.

(25) Zhao, Z.; Pu, X.; Han, C.; Du, C.; Li, L.; Jiang, C.; Hu, W.; Wang, Z. L. Piezotronic Effect in Polarity-Controlled GaN Nanowires. *ACS Nano* **2015**, *9*, 8578−8583.

(26) Zhou, R.; Hu, G.; Yu, R.; Pan, C.; Wang, Z. L. Piezotronic Effect Enhanced Detection of Flammable/Toxic Gases by ZnO Micro/Nanowire Sensors. *Nano Energy* **2015**, *12*, 588−596.

(27) Han, X.; Du, W.; Yu, R.; Pan, C.; Wang, Z. L. Piezo-Phototronic Enhanced UV Sensing Based on a Nanowire Photodetector Array. *Adv. Mater.* **2015**, *27*, 7963−7969.

(28) Xu, Q.; Yang, Z.; Peng, D.; Xi, J.; Lin, P.; Cheng, Y.; Liu, K.; Pan, C. $WS_2/CsPbBr_3$ van der Waals Heterostructure Planar Photodetectors with Ultrahigh on/off Ratio and Piezo-Phototronic Effect-Induced Strain-Gated Characteristics. *Nano Energy* **2019**, *65*, 104001.

(29) Liu, T.; Li, D.; Hu, H.; Huang, X.; Zhao, Z.; Sha, W.; Jiang, C.; Du, C.; Liu, M.; Pu, X.; Ma, B.; Hu, W.; Wang, Z. L. Piezo-Phototronic Effect in InGaN/GaN Semi-Floating Micro-Disk LED Arrays. *Nano Energy* **2020**, *67*, 104218.

(30) Sun, J.; Hua, Q.; Zhou, R.; Li, D.; Guo, W.; Li, X.; Hu, G.; Shan, C.; Meng, Q.; Dong, L.; Pan, C.; Wang, Z. L. Piezo-Phototronic Effect Enhanced Efficient Flexible Perovskite Solar Cells. *ACS Nano* **2019**, *13*, 4507−4513.

(31) Jiang, C.; Chen, Y.; Sun, J.; Jing, L.; Liu, M.; Liu, T.; Pan, Y.; Pu, X.; Ma, B.; Hu, W.; Wang, Z. L. Enhanced Photocurrent in InGaN/GaN MQWs Solar Cells by Coupling Plasmonic with Piezo-Phototronic Effect. *Nano Energy* **2019**, *57*, 300−306.

(32) Lu, J.; Yang, Z.; Li, F.; Jiang, M.; Zhang, Y.; Sun, J.; Hu, G.; Xu, Q.; Xu, C.; Pan, C.; Wang, Z. L. Dynamic Regulating of Single-Mode Lasing in ZnO Microcavity by Piezoelectric Effect. *Mater. Today* **2019**, *24*, 33−40.

(33) Yu, R.; Dong, L.; Pan, C.; Niu, S.; Liu, H.; Liu, W.; Chua, S.; Chi, D.; Wang, Z. L. Piezotronic Effect on the Transport Properties of GaN Nanobelts for Active Flexible Electronics. *Adv. Mater.* **2012**, *24*, 3532−3537.

(34) Zhang, S.; Ma, B.; Zhou, X.; Hua, Q.; Gong, J.; Liu, T.; Cui, X.; Zhu, J.; Guo, W.; Jing, L.; Hu, W.; Wang, Z. L. Strain-Controlled Power Devices as Inspired by Human Reflex. *Nat. Commun.* **2020**, *11*, 326.

(35) Milano, G.; Luebben, M.; Ma, Z.; Dunin-Borkowski, R.; Boarino, L.; Pirri, C. F.; Waser, R.; Ricciardi, C.; Valov, I. Self-Limited Single Nanowire Systems Combining All-in-One Memristive and Neuromorphic Functionalities. *Nat. Commun.* **2018**, *9*, 5151.

(36) Ielmini, D.; Zhang, Y. Analytical Model for Subthreshold Conduction and Threshold Switching in Chalcogenide-Based Memory Devices. *J. Appl. Phys.* **2007**, *102*, 054517.



https://dx.doi.org/10.1021/acs.nanolett.0c00733
*Nano Lett.* 2020, 20, 3761−3768

(37) Chen, Y.; Song, H.; Jiang, H.; Li, Z.; Zhang, Z.; Sun, X.; Li, D.; Miao, G. Reproducible Bipolar Resistive Switching in Entire Nitride AlN/n-GaN Metal-Insulator-Semiconductor Device and Its Mechanism. *Appl. Phys. Lett.* **2014**, *105*, 193502.
(38) Fu, K.; Fu, H.; Huang, X.; Yang, T.; Chen, H.; Baranowski, I.; Montes, J.; Yang, C.; Zhou, J.; Zhao, Y. Threshold Switching and Memory Behaviors of Epitaxially Regrown GaN-on-GaN Vertical P-N Diodes with High Temperature Stability. *IEEE Electron Device Lett.* **2019**, *40*, 375−378.
(39) Wu, W.; Wu, H.; Gao, B.; Deng, N.; Yu, S.; Qian, H. Improving Analog Switching in HfOx-Based Resistive Memory With a Thermal Enhanced Layer. *IEEE Electron Device Lett.* **2017**, *38*, 1019−1022.
(40) Kim, S.; Du, C.; Sheridan, P.; Ma, W.; Choi, S.; Lu, W. D. Experimental Demonstration of a Second-Order Memristor and Its Ability to Biorealistically Implement Synaptic Plasticity. *Nano Lett.* **2015**, *15*, 2203−2211.
(41) Sinclair, D. C.; Adams, T. B.; Morrison, F. D.; West, A. R. $CaCu_3Ti_4O_{12}$: One-Step Internal Barrier Layer Capacitor. *Appl. Phys. Lett.* **2002**, *80*, 2153−2155.
(42) Ohno, T.; Hasegawa, T.; Tsuruoka, T.; Terabe, K.; Gimzewski, J. K.; Aono, M. Short-Term Plasticity and Long-Term Potentiation Mimicked in Single Inorganic Synapses. *Nat. Mater.* **2011**, *10*, 591−595.


https://dx.doi.org/10.1021/acs.nanolett.0c00733
*Nano Lett.* 2020, 20, 3761−3768